

**APPENDIX E: Hydroclimatic reconstructions in the Lower Basin:
Water year precipitation reconstruction of the Muddy watershed**

by Kiyomi Morino and David Meko,
Laboratory of Tree-Ring Research, The University of Arizona

Table of Contents

E.1 Introduction	2
E.2 Study Basin.....	2
E.3 Data.....	2
E.3.2 Precipitation Data	2
E.3.3 Tree-Ring Data.	2
E.4 Methods	3
E.4.1 Reconstruction Model	3
E.5 Results and Discussion.....	3
E.5.1 Reconstruction modeling.....	3
E.5.2 Reconstructed precipitation.....	4
E.6 Conclusions	4
TABLES	5
Table E-1. List of site chronologies.....	5
Table E-2. Chronology basic statistics.....	6
Table E-3. Summary of single-site loess models.....	7
Table E-4. Summary of sub-period reconstruction models.	8
FIGURES	9
Figure E-1. Monthly basin precipitation.....	9
Figure E-2. Site map.	10
Figure E-3. PC loadings.....	11
Figure E-4. Agreement of observed and reconstructed precipitation.	12
Figure E-5. Time plots of annual reconstructed precipitation.	13

E.1 Introduction

The period of overlap between the streamflow and tree-ring data is about 30 years, too short to provide a robust calibration of the reconstruction models. Exploratory comparisons between individual candidate sites and both water year and winter, October through April, precipitation indicated a slightly stronger association with water year precipitation. This hydroclimatic variable was subsequently targeted for reconstruction.

E.2 Study Basin

The Muddy River watershed is comprised of three sub-watersheds: the Muddy (HUC: 15010012), the White (HUC: 15010011) and Meadow Valley Wash (HUC: 15010013). The total area drained by these three basins is 18,712 km². At the Muddy River near Glendale USGS gage (USGS ID: 09419000), the mean daily discharge for water years over the period of record (1950-2011) is 1.19 cms (42.2 cfs) (USGS 2012d). The highest water year mean was 2.04 cms (72.2 cfs) in 2005; the lowest was 0.86 cms (30.4 cfs) in 1997. Average water year runoff is 37.70 mcm (30.56 kaf).

E.3 Data

E.3.2 Precipitation Data

Precipitation data were derived from PRISM (Precipitation-elevation Regressions on Independent Slopes Model) data (Gibson et. al 2002). Monthly PRISM data, 1900-2010, for the continental US were downloaded from the PRISM site (<http://prism.oregonstate.edu/products/>). Data pertaining to the Muddy watershed were “clipped” from the larger dataset using a script written in MatLab™. Average precipitation depth in mm over the entire basin was computed. Precipitation is slightly bi-modal with the winter contribution to annual precipitation far exceeding the summer contribution (Figure E-1).

E.3.3 Tree-Ring Data.

Tree-ring data for this reconstruction consisted of measured ring-widths. These were obtained from the International Tree-Ring Data Bank (ITRDB) (<http://www.ncdc.noaa.gov/paleo/treering.html>) and from new sites collected not yet submitted to the ITRDB (Table E-1). The reconstruction developed in this study made use of 11 tree-ring chronologies, from an initial pool of 15 sites in or near the basin. Sites were selected with the criteria that the species be moisture-sensitive and the data cover at least the period 1700-1964. The 1700 cutoff ensured that at least two centuries of reconstructed streamflow data could be later analyzed for patterns of temporal variability; the 1964 cutoff ensured a reasonably long period (64 years) for calibration of precipitation with tree rings in the reconstruction model.

See *Hydroclimatic Reconstructions in the Lower Basin of the Colorado River, METHODS* for details regarding tree-ring data standardization.

Following chronology development, both WY and winter, October through April, precipitation were compared to tree-ring data using simple correlation analysis. Water

year precipitation showed a slightly stronger association with the tree-ring data and was targeted for reconstruction.

E.4 Methods

E.4.1 Reconstruction Model

See *Hydroclimatic Reconstructions in the Lower Basin of the Colorado River, METHODS* for details regarding methods employed in single-site reconstructions.

E.5 Results and Discussion

E.5.1 Reconstruction modeling

Tree-Ring Chronology Development

The reduced set of 11 tree-ring chronologies passing the screening for sample depth and correlation with flow are listed in Table E-1. Their site locations are marked by shaded triangles on the map in Figure E-2. The common period is 1612-1964, though some extend to earlier and later years. Exploratory correlation analysis pointed to 1500 as a feasible start year for reconstruction. All chronologies were therefore truncated to start in either 1500 or the first year with adequate subsample signal strength ($SSS > 0.85$). Descriptive statistics showed that the chronologies have near-zero autocorrelation and negative skew (Table E-2). The near-zero autocorrelation is expected, as these are residual chronologies (Cook et al. 1990b).

Single-Site Reconstruction

The SSR models explain 12-47 percent of the variance of precipitation in the calibration period, which ranges in length from 64 to 84 years for the 11 sites (Table E-3). Calibration periods start with 1901 but end in different years (1964 to 1984) depending on the collection date of the chronology. All models have some skill of verification, as indicated by an RE-statistic above zero.

The final selected smoothing parameter, α , for the SSR models ranges from 0.25 to 0.75. The variation in selected α reflects differences in curvature of the statistical relationship between precipitation and tree-ring index. Higher values indicate a more linear relationship.

Recalibration and Reconstruction

Summary statistics of the loess models used to recalibrate the scores of PC#1 of the SSRs into final estimates of winter precipitation are listed in Table E-4. The percentage of precipitation variance explained by the models ranges from 43 percent for Model A to 55 percent for Models B and C. All three models have positive skill, reflected by positive RE statistics for cross-validation, and the root-mean-square error increases only slightly (<10 percent) from the calibration to the validation data. Figure E-3 shows the PC#1 loadings for each of the models. Two pinyon sites, Panaca Summit and Moody Mountain, show the highest loadings for Model B.

Uncertainty

The validation statistics mirror the calibration R^2 in supporting the superior accuracy of Model B over the other two models (Table E-4). Statistics for Model B are most relevant, as that model supplies most of the reconstructed precipitation values. The RMSE of cross-validation of Model B is 40.0 mm (1.6 in), which is almost three-quarters of the standard deviation of water year precipitation for the 1901-1964 calibration period of the model.

E.5.2 Reconstructed precipitation

Water Year precipitation

Reconstructed winter precipitation, 1523 - 1982, is plotted in Figure E-5A along with a baseline at the long-term median of 237 mm (9.3 in) to facilitate identification of wet years and dry years. Reconstructed precipitation has a mean of 238 mm (9.4 in), is positively skewed (skew = 0.29, $p < 0.01$), not significantly autocorrelated ($r_1 = -0.053$, $p > 0.05$), and comparable to PRISM data, whose 1901-1982 mean is 248 mm (9.8 in).

There are two outstanding dry periods in this reconstruction: the late 1800s and mid-1600s (Figure E-5B). In both cases, maximum frequency of dry years in a 30-year window is about two-thirds. The maximum dry-year frequency in both periods exceeds the maximum frequency of dry years during the instrumental period. Several equally wet periods occur through the reconstruction, including two that immediately precede the dry periods just discussed. Other wet periods include one in the late 1600s and another in the mid-1700s.

E.6 Conclusions

The period of overlap between streamflow and tree-ring data was deemed too short to yield a robust reconstruction; instead, water year precipitation was reconstructed. Regression models showed moderate to good skill in tracking basin-wide, winter precipitation. Up to 55 percent of the variance was explained with the tree-ring data. The reconstruction identified the mid-1600s and late 1800s as particularly dry periods in the 500-plus year record.

TABLES

Table E-1. List of site chronologies.

N ¹	Site ²	Species ³	Location ⁴			Period ⁵
			Lat	Lon	El (m)	
1	Duck Crk Range	PIMO	39.3	-114.8	2286	1570-1976
2	Moody Mtn	PIMO	39.1	-115.8	2004	1470-1982
3	Panaca Summit	PIMO	37.8	-114.2	2103	1556-1982
4	Charleston Pk H-17	PILO	39.3	-115.6	3048	966-1964
5	Big Wash East	PIED	38.9	-114.2	2090	1612-1964
6	Sawmill Canyon	ABCO	36.7	-115.2	2743	1605-1977
7	Egan Range West	PIMO	39.4	-114.9	2134	1465-1976
8	Berry Crk	PIMO	39.4	-114.7	2242	1551-1976
9	Charleston Pk	PILO	38.9	-114.2	3425	800-1984
10	Spring Mountains	PILO	36.3	-115.7	3000	320-1984
11	Little Wolf Pass	PIED	36.8	-113.7	1800	1546-1971

1 Site number

2 Site name

3 Species code: PIMO is *Pinus monophylla*; PILO is *Pinus longaeva*; PIED is *Pinus edulis*; ABCO is *Abies concolor*

4 Latitude and longitude in decimal degrees, elevation in m above sea level

5 Start and end year of chronology, after trimming as described in text

Table E-2. Chronology basic statistics

N	Length ¹	Mean	Stdev	Skew ²	Replication and Common Signal ⁴			
					r(1) ³	#Cores	SSS	EPS
1	343(157)	0.993	0.240	-0.19	-0.02	4-37	0.88	0.86-0.98
2	460(179)	0.995	0.222	-0.24*	-0.01	4-36	0.85	0.83-0.98
3	322(150)	0.999	0.263	-0.21	-0.08	3-38	0.86	0.83-0.97
4	488(155)	0.995	0.231	0.24*	-0.09*	5-14	0.89	0.81-0.92
5	322(155)	0.995	0.214	-0.16	-0.02	5-18	0.86	0.78-0.93
6	295(155)	1.006	0.299	-0.29*	-0.05	3-26	0.89	0.87-0.98
7	373(177)	1.001	0.252	-0.17	-0.07	3-26	0.85	0.82-0.97
8	346(162)	0.997	0.230	-0.19	-0.02	3-26	0.86	0.82-0.97
9	957(177)	1.001	0.118	-0.16*	-0.09**	9-47	0.87	0.84-0.96
10	1225(161)	0.998	0.230	-0.03	-0.07*	10-36	0.96	0.93-0.98
11	376(161)	1.007	0.216	-0.26*	-0.05	3-18	0.85	0.82-0.96

1 Length of site chronology, with minimum segment length in parentheses

2 Skewness (*, ** denote significance at 0.05, 0.01 level)

3 First-order autocorrelation (*, ** denote r(1) significantly different from zero at 0.05, 0.01 level)

4 Range in number of cores, minimum value of subsample signal strength, and range in expressed population signal

Table E-3. Summary of single-site loess models.

N ¹	Calibration ²				Validation ³		
	Period	α	V	RMSE	RE	RMSE	Group ⁴
1	1901-1976	0.65	0.24	49.1	0.17	51.8	B
2	1901-1982	0.65	0.37	48.8	0.32	51.1	ABC
3	1901-1982	0.25	0.47	44.5	0.39	48.7	BC
4	1901-1964	0.60	0.23	48.4	0.17	51.1	AB
5	1901-1964	0.75	0.30	46.1	0.25	48.7	B
6	1901-1977	0.60	0.33	45.5	0.28	48.1	
7	1901-1976	0.70	0.29	47.3	0.22	50.2	B
8	1901-1976	0.35	0.28	47.5	0.19	51.2	B
9	1901-1984	0.60	0.14	59.1	0.08	62.0	ABC
10	1901-1984	0.90	0.12	60.0	0.08	61.9	ABC
11	1901-1971	0.75	0.38	43.4	0.34	45.4	B

1 Site number, as in Table 1

2 Calibration statistics: N=period for estimation of loess curve,
 α =loess smoothing parameter, V=variance-explained decimal fraction,
 RMSE=root-mean-square error of calibration

3 Validation statistics from leave-1-out cross-validation:
 RE=reduction of error statistic, RMSE=root-mean-square error

4 Subperiod reconstruction groups, see Table 4

Table E-4. Summary of sub-period reconstruction models.

N ¹	Period ²	p ³	Calibration ⁴			Validation ⁵	
			α	V	RMSE	RE	RMSE
A	1523-1964	4	0.35	0.43	41.5	0.33	45.8
B	1661-1964	10	0.40	0.55	37.0	0.49	40.0
C	1661-1982	4	0.30	0.55	41.2	0.47	45.3

1 Sub-period model name

2 Starting and ending years of sub-period

3 Number of chronologies

4 Calibration statistics: α =loess smoothing parameter,
V=variance-explained decimal fraction, RMSE=root-mean-square
error of calibration

5 Validation statistics from leave-1-out cross-validation:
RE=reduction of error statistic, RMSE=root-mean-square error

FIGURES

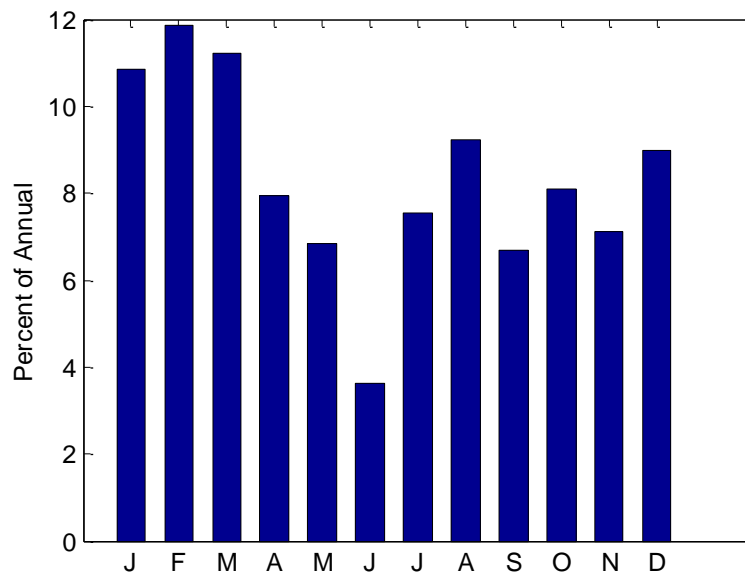


Figure E-1. Monthly basin precipitation.

Bar charts summarizing annual distribution of monthly basin precipitation, 1900-2010. Data from PRISM.

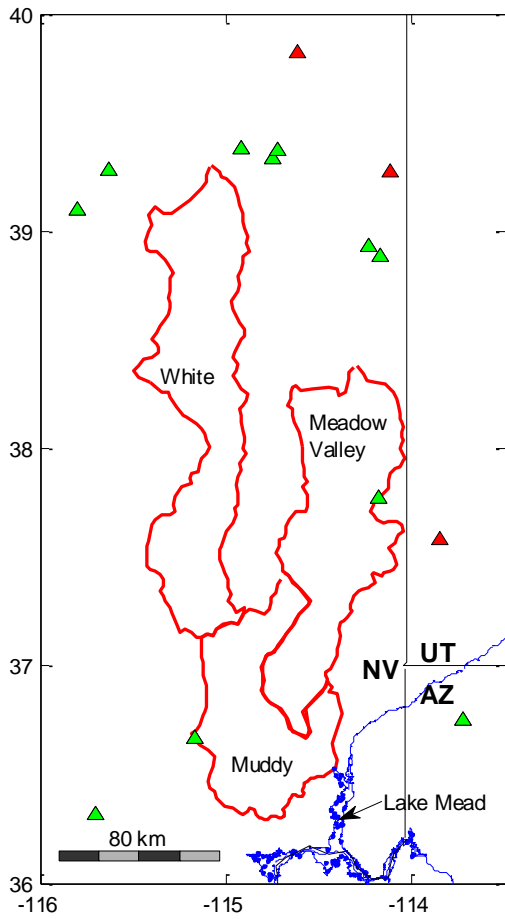


Figure E-2. Site map.

Map showing tree-ring site locations. Tree-ring sites that passed initial screenings are denoted by green triangles. Tree-ring sites that did not pass screenings are denoted by red triangles.

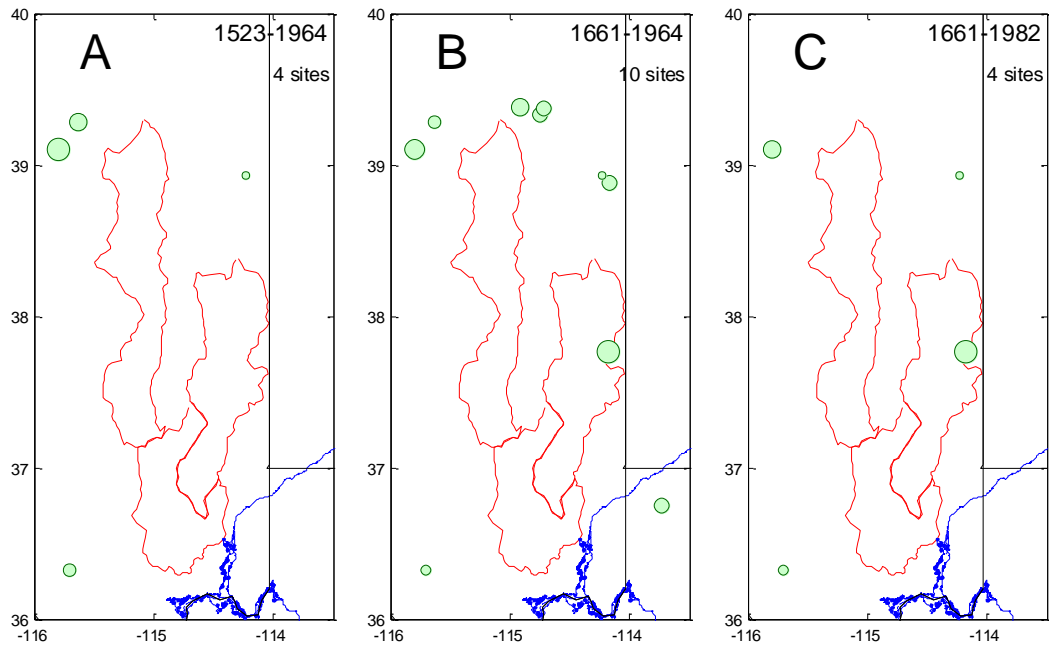


Figure E-3. PC loadings.

Tree-ring site locations for sub-period reconstruction models. Models A, B and C coded as in Tables 4. Symbol sizes reflect magnitude of loadings of sites on PC#1 of SSRs.

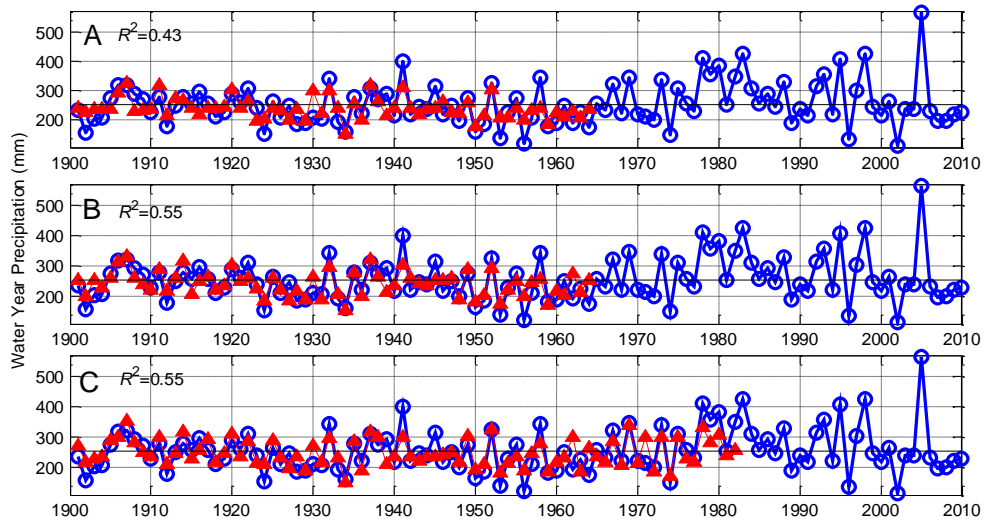


Figure E-4. Agreement of observed and reconstructed precipitation.

Agreement of observed and reconstructed precipitation for three sub-period models (as coded in Table 4). Annotated at upper left is the variance explained by the model. Horizontal line is the observed mean precipitation for the period, 1900-2010.

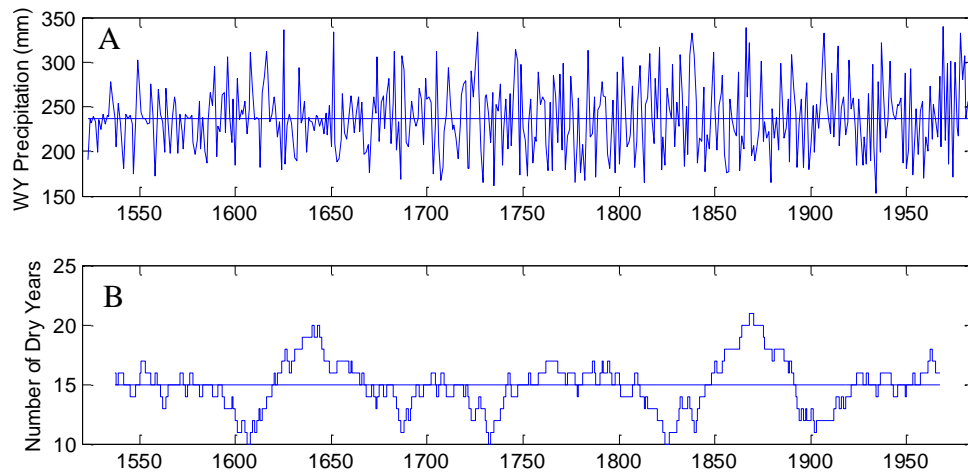


Figure E-5. Time plots of annual reconstructed precipitation.

Time plots of annual reconstructed years and dry-year frequency. (A) Reconstructed precipitation, 1496-2010, and dry year threshold (horizontal line) at median. (B) Frequency of dry years in centered 30-year moving window. Horizontal line in (B) is expected number of dry years in 30-year window.